JOURNAL OF MARITIME RESEARCH

Vol XXIII. No. I (2026) pp 144–156

ISSN: 1697-4840, www.jmr.unican.es

Chloride transport accelerated via modest electromigration as a means to initiate corrosion of the steel reinforcement

Kazi Naimul Hoque[1,*], Francisco Presuel-Moreno[2]

ARTICLE INFO

Article history:
Received 11 Apr 2025;
in revised from 15 Apr 2025;
accepted 18 May 2025.

Keywords:
Accelerated chloride transport, Reservoir length, Fly ash, Slag, Silica fume, Corrosion current.

ABSTRACT

Specimens with binary (SL, FA) and ternary (T1, T2) concrete mixes (30.5 cm x 12.7 cm x 7.6 cm) were prepared without any chlorides, using a w/cm ratio of 0.41 or lower. Each specimen, reinforced with #3 rebar, have a 0.75 cm concrete cover. The specimens had reservoirs of varying lengths on their top surface. A 10% NaCl solution by weight was introduced into the reservoirs, and electromigration was applied for a period ranging from few weeks to several months to accelerate chloride transport. Corrosion current values were monitored for approximately 1600 days using galvanostatic pulse techniques and converted to mass loss using Faraday's law. The SL mix specimens showed the highest average corrosion current values, followed by FA, T1, and T2 mix specimens. Despite the prolonged exposure, no visible corrosion such as cracks or surface-reaching corrosion products were observed over the monitoring period.

1. Introduction.

Steel corrosion in concrete is a major cause of degradation in steel reinforced concrete (RC) structures [1-3]. It is mostly caused by carbonation or chloride ingress. Chloride-induced corrosion is thought to be more harmful than carbonation - induced corrosion [4]. Regardless of whether steel corrosion is caused by chloride or carbonation, the natural rate of advancement is generally slow, making it difficult to produce relevant findings for decision-making. The situation is worsened by the fact that there are very few research and results on natural corrosion initiation and propagation [5-11]. These investigations reveal that significant corrosion-induced damage in RC structures experiencing natural corrosion requires rather extended monitoring time periods which depend on concrete cover and concrete compositions.

Accelerated corrosion tests are used to simulate the steel corrosion process and predict corrosion-induced damage (e. g. loss of steel-concrete interface bond, cover cracking, spalling, loss of member stiffness [9, 12-17] has become a common practice today. 'Accelerated corrosion' of steel (in concrete) is a term that refers to a steel corrosion process that happens at a higher rate than its natural counterpart. When compared to natural corrosion, the impacts of accelerated corrosion (i.e., depassivation and/or corrosion-induced damage) can be observed in a shorter period. Accelerated corrosion approaches have previously been utilized to investigate the time to corrosion initiation and corrosion-induced damage in RC structures, as well as the impact on parameters such as deformation behavior, ductility, bond strength, and modes of failure [18-21]. With the present demand to measure and account for the corrosion propagation phase in the service life of corrosion-affected RC structures [7, 22, 23], there is a need to research and develop approaches that can reduce the time to corrosion initiation, while simulating natural corrosion propagation as closely as possible.

During the corrosion propagation stage of reinforcing steel embedded in concrete, the buildup of corrosion products (after they exceed a specific volume and reach a critical penetration) is known to cause cracks and finally spalls. Several studies have

[1]Department of Naval Architecture and Marine Engineering, Bangladesh University of Engineering and Technology (BUET), Dhaka, Bangladesh.

[2]Department of Ocean & Mechanical Engineering, Florida Atlantic University (FAU), Boca Raton, Florida, United States.

[*]Corresponding author: Kazi Naimul Hoque. E-mail Address: kazinaim@name.buet.ac.bd.

been conducted in which chlorides were introduced to the concrete mix of the specimens (to initiate corrosion immediately) and then a current was applied to accelerate the corrosion process taking place at the reinforcement [24-28].

The applied current's magnitude has sometimes been significant enough to induce cracks within a few days to weeks. Some studies [24,25, 29, 30] recommended using a current of 100 μA/cm^2 to mimic maximum-field values obtained, and in these studies the current was maintained for a few weeks to several months under these conditions. Other studies have examined how corrosion initiates and propagates when cracks of various sizes (incipient, 0.4, and 0.7 mm) are present [31-33].

To better understand the critical quantity of corrosion products that might induce a crack, Sagüés and collaborators [29, 30] investigated the influence of the length of the corroding site (assuming uniform corrosion around the corroding rebar length), rebar diameter, and concrete cover. The chlorides were added to the concrete mix when the specimens were prepared [29, 30]. In the field, chloride ions penetrate from the surface toward the reinforcement in partially submerged bridges exposed to a marine environment. As a result, the side of the rebar exposed to the chlorides would be the first to reach the chloride threshold and initiate corrosion. The first corrosion site(s) might be as little as a small pit (i.e., < 1 mm diameter). Once corrosion has initiated, it is expected that the corroding site(s) will exert corrosion protection on the surrounding steel region (the throwing power of which will depend on the concrete resistivity and moisture content), causing the next corroding site to be some distance away from the first [29, 30]. After some time, it is likely that as corrosion progress the corroding sites could coalesce.

Four different concrete compositions were prepared for this study. The length of the solution reservoir was used as an attempt to alter the length of the anode. The chloride transport into the concrete was accelerated by electromigration. The method was developed using findings from prior research [34-36]. With this methodology, the corrosion of the rebar usually begins after a few weeks or months. The galvanostatic pulse (GP) measurements were used to monitor the corrosion progression stage. Accounting for nearly 1600 days, the corrosion current and mass loss values were monitored.

2. Experimental details.

2.1. Concrete mixes, casting and curing of specimens.

Reinforced concrete samples were prepared in 2016. In April 2016, two sets of samples were prepared (binary mixes with Fly Ash (FA) or Slag (SL)). During August 2016, two more sets of samples were prepared (ternary mixes, see Table 1). Three concrete mixes were prepared with a w/cm ratio of 0.41 and the other concrete mix was prepared with a w/cm ratio of 0.37. The concrete mixes are detailed in Table 1. Additional details of each concrete mixes can be found in the reference [37].

Table 1: Concrete mix detail for SL, FA, T1 and T2 specimens.

Concrete Mix	Cementitious Content	Cement Content	20% FA	8% SF	50% Slag	Fine agg.	Coarse agg.	w/cm ratio
	(kg/m^3)	(kg/m^3)	(kg/m^3)	(kg/m^3)	(kg/m^3)	(kg/m^3)	(kg/m^3)	
SL	390	195	0	0	195	782	1009	0.41
FA	390	312	78	0	0	967	833	0.41
T1	390	117.5	78.3	0	195.2	761	1009	0.41
T2	390	289	70	31	0	790	1046	0.37

Source: Authors.

These single rebar sections have a radius of 0.47 cm i.e., #3 rebars Rebar segments were cut to size, with about 4 cm protruding outside of the concrete. The rebars were wired brushed. The reinforcement was cleaned with hexane prior to casting to remove any grease. Figure 1 depicts three molds for single rebar samples. The dimensions of these single rebar specimens were 30.5 cm x 12.7 cm x 7.6 cm (12 in x 5 in x 3 in). For mixes, SL and FA eleven single rebar specimens were prepared per mix with a concrete cover of 0.75 cm (0.3 in). During the casting that took place on August 19, 2016, five (T1) or six (T2) single rebar specimens were prepared per concrete mix with a concrete cover of 0.75 cm as well. Before casting the concrete, each rebar was tapped on one end and a stainless-steel screw was placed (i.e., each rebar was drilled and tapped). This procedure was completed to establish an electrical contact for corrosion monitoring.

Figure 1: Some single rebar molds with reinforcement prior to casting.

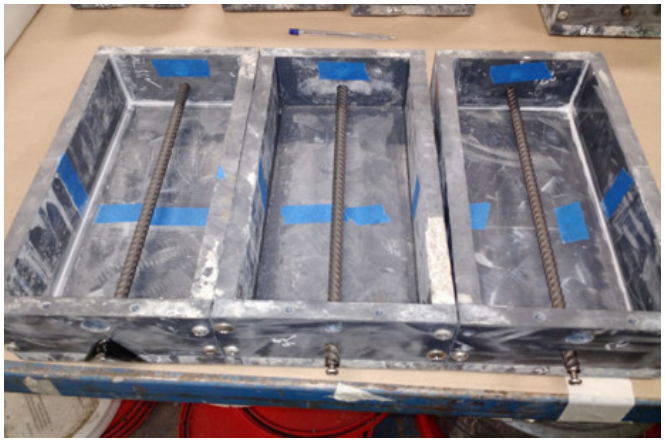

Source: Authors.

At casting, all specimens had stainless steel (or titanium mix metal oxide 'TiMMO') mesh embedded on the top side. During the experiment, this surface became the bottom surface. The mesh was used as an electrode used to accelerate chloride transport, (see next section). Meshes ranged in length from 2.5 cm to 17.5 cm and were about 3 cm wide and were positioned along the central portion of the rebar. The specimens were made at the Florida Department of Transportation's State Materials Office (SMO). The molds were removed after one day and brought

to the fog room for curing for at least 28 days.

2.2. Specimen setup preparation for electromigration.

These samples were transported to FAU SeaTech campus for the next phase of the experiment around the end of May 2016 for SL & FA mixes and towards the middle of October for T1 & T2 mixes. Upon arrival at FAU-SeaTech, these samples were stored in a high humidity chamber until the solution reservoir was installed, this allow the concrete to continue curing. The samples were subsequently transferred to the laboratory environment (65% RH and 21°C) for at least a couple of days prior to installing the solution reservoir for ponding.

Figure 2: Four single rebar specimens with reservoirs installed.

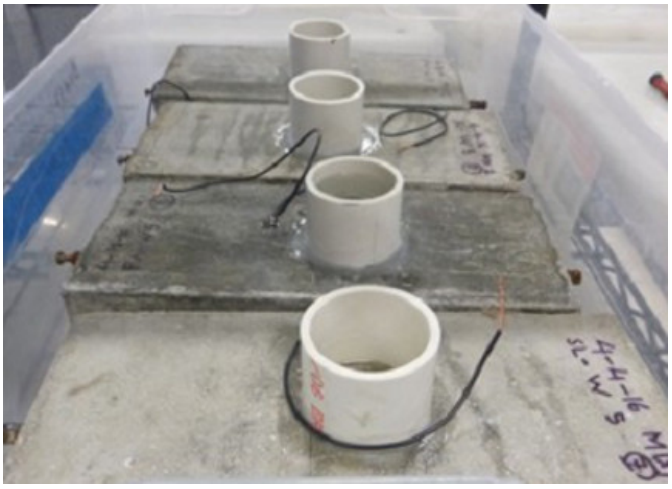

Source: Authors.

Using marine grade adhesives, a plastic reservoir was affixed to the top surface (which was the mold surface during casting). The reservoir was installed at least 40 days after casting. NaCl solution was poured into the reservoir (10% NaCl-by weight). The goal was to have different corroding lengths. Hence, the area where corrosion could initiate was constrained to some extent by the reservoir length. On the top surface of the concrete samples, each reservoir was centered along the rebar length. The length of the ponding ranged from 2.5 cm to 17.5 cm. Figure 2 depicts four single rebar samples after the solution reservoirs have been placed but before the solution has been filled. Prior to the following procedure, the samples were kept in high humidity for 3 to 7 days. Electrodes (stainless steel wire mesh or TiMMO mesh) with similar sizes that those embedded were placed on the top surface inside the solution reservoir.

Samples were kept in transparent plastic containers. Each specimen was partially submerged in a saturated calcium hydroxide solution, with about one centimeter of the concrete specimen immersed. Each sample was placed on top of a white plastic mesh (acrylic perforated). This procedure was used to reduce the amount of leaching from the concrete during the electromigration.

2.3. Electromigration.

A power supply was used to set a potential hold between the top and bottom mesh. The chlorides in the solution above each rebar are then driven into the concrete and towards the embedded rebar by an electric field. The electrode in the NaCl solution was connected to the power supply's negative terminal. The positive terminal of the power supply was connected to the embedded mesh in each specimen. To minimize direct contact between the titanium mix metal oxide wire mesh and the concrete surface, an acrylic mesh was placed in the solution reservoir. The experimental setup used for electromigration is shown in Fig. 3.

Figure 3: Experimental setup used for electromigration.

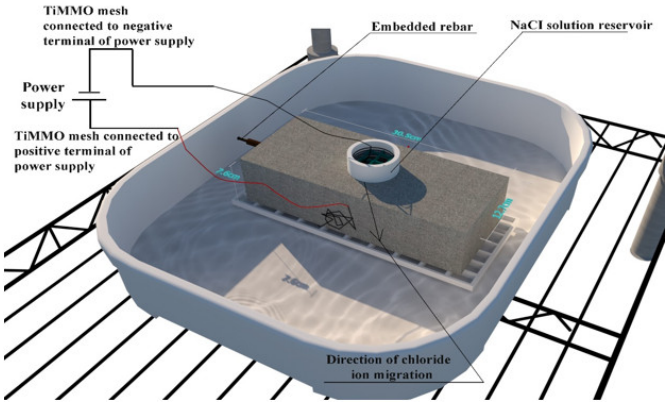

Source: Authors.

Table 2: Single rebar samples made with slag replacement.

Sample Name	Reservoir Length (cm)	Total Ampere Hour	Duration (days)
SL-1	17.5	1.701	27
SL-2		1.47	50
SL-3		3.162	16
SL-4	2.5	3.66	54
SL-5		3.701	82
SL-6	5	4.016	84
SL-7		2.482	64
SL-8		2.351	84
SL-9	10	4.282	82
SL-10		2.369	55
SL-11		3.438	49

Source: Authors.

Table 2, Table 3, and Table 4 show how each sample was labeled. Each of these tables also includes the sample name/ID, reservoir length, and the duration of electromigration periods. There is also a column in Tables 2 and Table 3 that displays the calculated Ampere-hour applied (integrated values), this gives a better sense of the charge that the electric field applied. Specimens made using ternary blends were labeled in a similar manner. The labels for the samples made using ternary concrete

mixes are shown in Table 4. Several electromigration durations were applied to each specimen between the start and end dates.

Table 3: Single rebar samples made with fly ash replacement.

Sample Name	Reservoir Length (cm)	Total Ampere Hour	Duration (days)
FA-1	5	4.069	84
FA-2		3.015	74
FA-3		1.718	16
FA-4	7.5	5.889	16
FA-5		3.524	25
FA-6		3.729	30
FA-7	17.5	8.145	64
FA-8		6.942	74
FA-9		6.676	65
FA-10	2.5	2.742	64
FA-11		3.531	73

Source: Authors.

Initially, electromigration was performed on all single rebar SL and FA specimens. The delta potential across a 100 ohms' resistor was used to determine the amount of current being applied when a particular potential difference was supplied for several days at a time. The system was turned off at regular intervals and the rebar potential was measured with respect to a saturated calomel reference electrode during the disconnected period. Although the rebars were not an electrode in the system, the rebars were polarized by an ionic current produced by the applied electric field.

Table 4: Single rebar samples made with T1 or T2 mixes.

Sample Name	Reservoir Length (cm)	Total Ampere Hour	Duration (days)
T1-7	5	0.56	21
T1-10		0.665	30
T1-9	10	0.565	21
T1-6	15	0.612	19
T1-8		0.665	30
T2-1	5	0.578	21
T2-3		0.654	30
T2-5		0.654	30
T2-4	10	0.536	19
T2-2	15	0.654	30
T2-11		0.771	21

Source: Authors.

If the previous rebar potential measured revealed that corrosion had not initiated, the electromigration was restarted after monitoring the rebar potential for some time with the system being disconnected (typically at least 2 hours, but in some cases it lasted several days). The electromigration process was maintained until the specimen revealed an off-rebar potential, which might indicate the start of corrosion in that embedded rebar (a value of -0.200 Vsce or more negative was used in here). In most instances, the rebar potential after corrosion initiation was more negative than -0.200 Vsce. A potential value of -0.150 Vsce (~ -0.220 V vs. CSE) has been reported [34] as a value at which corrosion initiates on lab specimens not previously corroding.

As stated previously, the samples were energized at different times. For the initial samples, the applied potential was 9 V. When monitoring rebar potential vs. a saturated calomel reference electrode (SCE) while the electric field was still on, a potential larger than +2Vsce was detected (which could cause pitting to initiate at low chloride concentration), thus the applied potential was decreased to 3 V. The rebar potential readings were taken with the power supply on, a few seconds after turning the power supply off, and rebar off potentials after one hour and two-hour intervals, in a manner similar to a depolarization test. The decision was then made to either turn off the electromigration or restore the applied potential (i.e., electromigration back on). The system was switched off for two days or longer after selected disconnections, and then LPR and EIS measurements were performed. In certain cases, the system was turned off for a longer period, the rebar potential was monitored, and electromigration was resumed if the rebar potential had moved to values more positive than -0.200 Vsce. In some cases, electromigration was stopped prior to meeting these criteria. It is to mention that the natural chloride diffusion took place during the subsequent monitoring period. Details of the results can be found in reference [37].

3. Electrochemical measurements after initiation of corrosion.

Using a saturated calomel reference electrode and a high impedance voltmeter, the rebar potential was monitored at regular intervals during the corrosion propagation stage, i.e., after the electromigration. Electrochemical characterization using LPR and EIS took place during the early monitoring stage, the results are reported in these reference [37].

After six months following the electromigration phase, GP tests were conducted. This test technique provided an alternative approach of determining Rs and Rc values. The GP measurements were performed about once a month during the corrosion propagation stage. Initially, a galvanostatic pulse of 10 μA was used (but later, the applied current was adjusted, when necessary to keep the polarization to less than 25 mV from the instant on value, i.e., the ΔV between the value after 0.2 seconds and the last on value of the test). For the initial set of measurements, 140 seconds were used. During the second set, the GP duration was increased to 300 seconds because the slope of the curve in some rebars was still changing at 140 seconds (according to theory constant slope is needed to determine Rc). As a compromise, all subsequent testing was conducted for 200 seconds. The device used for the GP test measures the open circuit potential for a few seconds first. The rebar potential is

then measured as a function of time after the pulse is applied in intervals of 0.2 milliseconds. Using the rebar potential prior to the GP and the first potential reading with the current pulse (i.e., the initial on-potential), the Rs(GP) was determined. The difference between the initial on-potential and the rebar on-potential value obtained at 200 seconds and the applied current was used to determine the Rc(GP).

The Rc values obtained from GP readings were converted to corrosion current (Icorr) values as the corroding area is unknown. The corrosion current values were then converted to mass loss using Faraday's law calculations. The Icorr was determined using the Stern-Geary equation i.e., Icorr = B/Rp where Rp is the polarization resistance (defined previously as Rc) and B is the Stern-Geary coefficient that ranged from 13 to 52 mV depending on the steel's corrosion condition (i.e., passive, or active). In the case of concrete, a value of 26 mV for corroding (active) steel and 52 mV for passive steel has been developed and employed by most researchers [38-40]. In here a value of 26 mV was chosen.

4. Results and Discussion.

4.1. Evolution of corrosion current from GP measurements.

The following section describes the evolution of Icorr over time obtained from GP measurements for different single rebar samples. Day zero for all the plots shown below refers to the day when the solution was added to the installed solution reservoir and not the age of the specimen. Not all solution reservoirs were filled at the same time, and hence the number of days from initial fill vary. For SL, FA, T1 and T2 single rebar samples, the Icorr plots correspond to the values obtained by using the GP method, throughout the monitored period of approximately 1600 days.

Figure 4: Icorr with time obtained from GP method on selected rebars (SL samples) under different size reservoir.

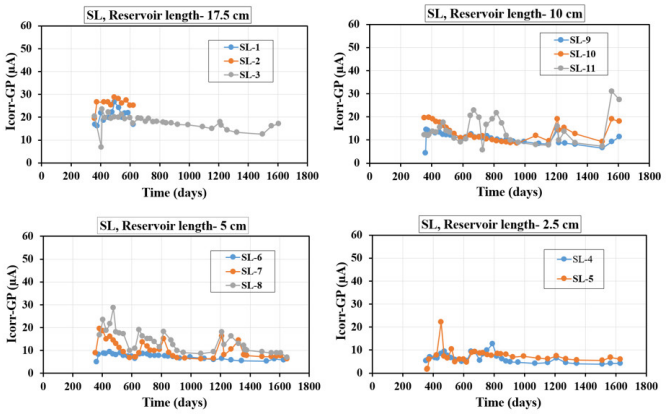

Source: Authors.

Fig. 4 depicts the evolution of Icorr with time obtained from GP method for single rebar SL samples under different size solution reservoir. In case of 17.5 cm solution reservoir size, it is observed that SL-1 and Sl-2 samples with Icorr values larger than 25 μA were terminated around 620 days, and Icorr values varied between 6.9-24.5 μA for SL-3 specimen (17.5 cm solution reservoir), with most values larger than 11 μA. For SL-3 sample, between day 400 and 600, Icorr was around 20 μA. After day 600, a monotonic decrease was observed (from 20 μA to 12 μA, two Icorr increases occurred one on day 1200 and the last two measurements returning close to 20 μA. While comparing the Icorr values measured on rebars of samples with 10 cm solution reservoir size, it is noticed that most of the samples showed fluctuations over time in terms of Icorr values, the most recent two set of readings showed an increase in corrosion activity (increased Icorr values), and values ranged from 4.4-32.2 μA when considering the whole period. For SL-10 sample, the current decrease from 20 μA to 9.5 μA by day 960, thereafter cyclic increases were observed, and the most recent readings showed Icorr values of more than 18 μA. For 5 cm solution reservoir size, it is seen that most of the samples showed a fluctuating trend in terms of corrosion current, except for SL-6 sample which gives a monotonically decreasing trend for the most period (with Icorr ranging between 8 μA and 10 μA). For SL-6 sample, all Icorr values were less than 10 μA. SL-7 and SL-8 samples had several cyclic periods (i.e., increase followed by a decrease), for the last 200 days the Icorr has been close to 10 μA. Icorr values ranged from 5.0-28.7 μA for these samples (5 cm solution reservoir). In case of 2.5 cm solution reservoir size, it is found that all the samples showed a slightly fluctuating trend in terms of Icorr values over time, corrosion current values were less than 10 μA for most of the period, and values ranged from 1.5-13 μA. In case of comparison, corrosion current values were higher for the samples having 17.5 cm solution reservoir size, corrosion current values were very much comparable for samples with 5 cm and 10 cm solution reservoir sizes respectively, while the corrosion current values were lower for the samples with 2.5 cm solution reservoir size. In addition, recent corrosion current values were very much comparable on selected SL single rebar specimens having 2.5 cm and 5 cm solution reservoir sizes respectively.

Figure 5: Icorr with time obtained from GP method on selected rebars (FA samples) under different size reservoir.

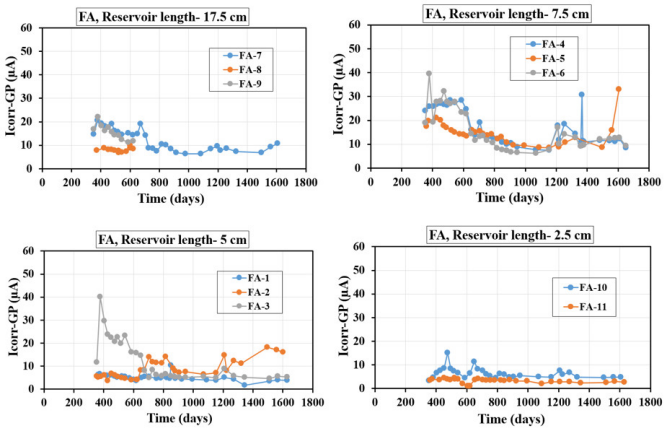

Source: Authors.

Fig. 5 highlights the evolution of Icorr with time obtained from GP method for single rebar FA samples under different size solution reservoir. In case of 17.5 cm solution reservoir size, it is observed that all the samples showed initially a downward trend in terms of Icorr values, but in the case of FA-7, the Icorr value plateau to a value close to 10 μA for the most recent periods, and for FA-8 sample which showed an Icorr close to 10 μA for most of the observed period. FA-8 and FA-9 samples were terminated around 620 days, and Icorr values varied from 6.4-22.1 μA for specimens having 17.5 cm solution reservoir size. While comparing Icorr values for rebars under 7.5 cm solution reservoir size, it is noticed that all the samples showed a downward trend in terms of Icorr values until 1160 days, followed by a fluctuating trend thereafter, and Icorr values ranged from 6.1-39.5 μA. FA-4 and FA-6 specimens showed an increase in Icorr values from 1100 to 1200 days, and after placing these specimens in the environmental chamber the Icorr values became smaller, but with a modest monotonic increase between day 1400 and day 1600. For 5 cm solution reservoir size, it is seen that all the samples showed a fluctuating trend in terms of Icorr over time, except for FA-1 sample which gives a plateau trend for most of the observed period, FA-2 sample showed an increase in Icorr values for the most recent 400 days, and Icorr values ranged from 1.7-40.2 μA for these specimens (5 cm solution reservoir). In case of 2.5 cm solution reservoir size, it is found that FA-10 sample showed a fluctuating trend, whereas FA-11 sample followed a monotonically decreasing trend for most of the observed period in terms of Icorr, and values varied from 1.0-15.2 μA for these specimens.

Figure 6: Icorr with time obtained from GP method on selected rebars (T1 samples) under different size reservoir.

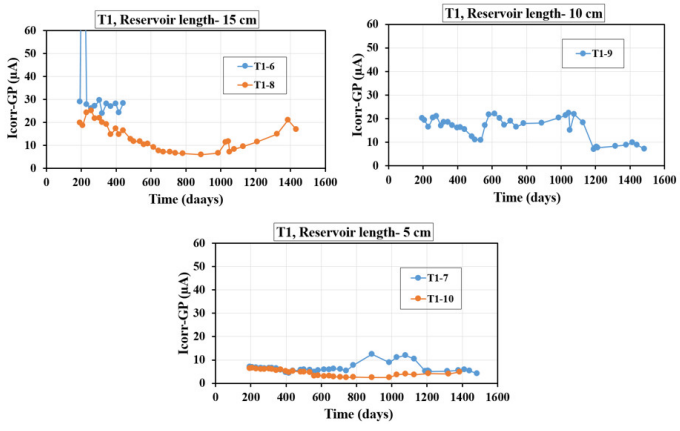

Source: Authors.

In case of comparison, corrosion current values were higher for the samples having 7.5 cm solution reservoir size, corrosion current values were very much comparable for specimens having 5 cm and 17.5 cm solution reservoir sizes respectively, while the corrosion current values were lower for the samples with 2.5 cm solution reservoir size. In addition, corrosion current values were very much comparable on selected rebars for 5 cm, 7.5 cm, and 17.5 cm solution reservoir sizes respectively, while it was comparable on selected rebars as well for 2.5 cm and 5 cm solution reservoir sizes respectively.

Fig. 6 illustrates the evolution of Icorr with time obtained from GP method for single rebar T1 samples under different size solution reservoir. In case of 15 cm solution reservoir size, it is observed that T1-6 sample showed a fluctuating trend over time in terms of Icorr (T1-6 sample has been terminated around 450 days), whereas T1-8 sample followed a downward trend until day 900 (Icorr was around 6 μA), after that a monotonic (almost exponential) increase has been observed with recent readings reaching 20 μA. Icorr values ranged from 5.9-30 μA for these specimens having 15 cm solution reservoir size. While observing 10 cm solution reservoir size, it is noticed that T1-9 sample showed a fluctuating trend over time, and Icorr values ranged from 7.0-22.3 μA. For 5 cm solution reservoir size, it is seen that both the samples T1-7 and T1-10 showed a monotonically decreasing trend until day 550, therefore T1-7 sample showed an upward trend and T1-10 sample showed a slightly downward trend. Icorr values for these samples ranged from 2.4-12.4 μA. In case of comparison, corrosion current values were higher for the samples having 15 cm solution reservoir size, whereas corrosion current values were lower for those samples with 5 cm solution reservoir size. In addition, corrosion current values were very much comparable for 5 cm and 15 cm solution reservoir sizes respectively, for some instances on selected samples.

Figure 7: Icorr with time obtained from GP method on selected rebars (T2 samples) under different size reservoir.

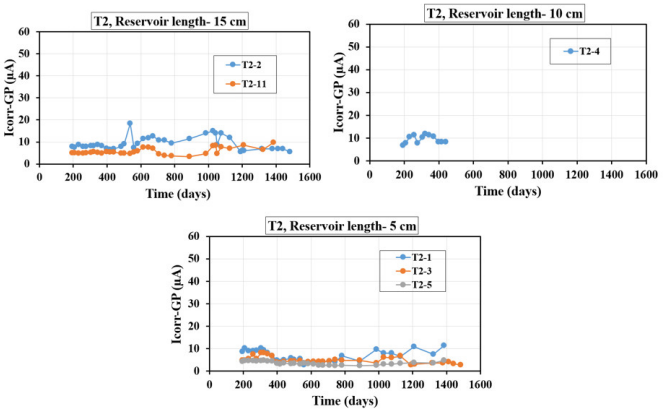

Source: Authors.

Fig. 7 describes the evolution of Icorr with time obtained from GP method for single rebar T2 samples under different size solution reservoir. In case of 15 cm solution reservoir size, it is noticed that both the samples (T2-2 and T2-11) showed fluctuating trend in terms of Icorr over time. It is interesting to note that T2-11 sample showed a modest increase in terms of Icorr, reading was 10 μA at day 1400, whereas from day 200 to day 600 Icorr ranged between 5 μA and 6 μA, similar for T2-2 sample in which Icorr value reached close to 10 μA at day 1420. Icorr values ranged from 3.4-15 μA for these specimens having 15 cm solution reservoir size. While looking at the Icorr plots for 10 cm solution reservoir size, it is found

that T2-4 sample showed a slightly fluctuating trend over time, and Icorr values ranged from 6.7-11.8 μA. This sample T2-4 was terminated around 450 days. For 5 cm solution reservoir size, it is observed that both the sample (T2-1 and T2-3) showed fluctuations in terms of Icorr over time, whereas T2-5 sample followed a monotonically decreasing trend for most of the period. Icorr values ranged from 2.4-10.8 μA for these samples having 5 cm solution reservoir size. In case of comparison, corrosion current values were comparable for 10 cm (T2-4) and 15 cm (T2-2) solution reservoir sizes respectively, on selected samples, whereas corrosion current values were comparatively lower for those samples with a 5 cm solution reservoir size. In addition, corrosion current values were very much comparable for 5 cm and 15 cm solution reservoir sizes respectively, on selected samples.

Tables 5 through Table 7 present the average Icorr values and standard deviations (STD) from the final 15 sets of measurements taken using the GP method for SL, FA, T1, and T2 concrete mixes containing a single rebar.

Table 5 presents the average Icorr and STD values from GP readings for SL single rebar specimens. Since SL-1 and SL-2 samples were terminated early, they lack comparable data to SL-3 sample. Notably, the highest average Icorr was found in SL-3 sample, which had the longest solution reservoir of 17.5 cm, with an average of 16.1 μA and an STD of 1.7 μA. In contrast, the lowest average Icorr was recorded for SL-4 sample, which had the smallest solution reservoir of 2.5 cm, with average and STD values of 5.6 μA and 2.3 μA, respectively. The largest STD of 6.8 μA was observed in SL-11 sample, while most samples had STD values around or below 3.0 μA.

Table 5: Average Icorr and STD values obtained from GP readings for SL single rebar specimens.

SL mix			
Sample Name	**Reservoir Length (cm)**	**Avg. Icorr (μA)**	**STD (μA)**
SL-1*	17.5	-	-
SL-2*		-	-
SL-3		16.1	1.7
SL-4	2.5	5.6	2.3
SL-5		7.0	1.0
SL-6	5	6.6	0.8
SL-7		9.0	3.0
SL-8		11.8	3.0
SL-9	10	9.4	1.8
SL-10		11.9	3.7
SL-11		13.6	6.8

Note: (*) stands for those specimens that had been terminated

Source: Authors.

Table 6 presents the average Icorr and STD values from GP readings for FA single rebar specimens. FA-8 and FA-9 samples had no recorded values due to early termination. The highest average Icorr was observed in FA-4 sample, with an average of 12.6 μA and an STD of 5.2 μA, corresponding to a 7.5 cm solution reservoir. The lowest average Icorr was found in FA-11 sample, which had a 2.5 cm reservoir, with average and STD values of 3.0 μA and 0.5 μA, respectively. FA-4 sample also had the largest STD value of 5.2 μA, while most samples had STD values below 3.0 μA.

Table 7 provides the average Icorr and STD values from GP readings for T1 and T2 single rebar specimens. T1-6 and T2-4 samples lack data as they were terminated early. For the T1 specimens, the highest average Icorr was found in T1-9 sample, with a reservoir length of 10 cm, showing an average value of 15.2 μA and an STD of 5.7 μA. The lowest average Icorr of T1 sample was in T1-10, with a 5 cm reservoir, having an average Icorr of 3.3 μA and an STD of 0.8 μA. In the T2 samples, the highest average Icorr was recorded in T2-2 (reservoir length of 15 cm) with an average value of 10.0 μA and an STD of 3.2 μA. The lowest value was observed in T2-5 sample, with a 5 cm reservoir, where the average Icorr and STD values were 3.0 μA and 0.7 μA, respectively. Although T1 and T2 samples had some larger STD values, 5.7 μA and 3.2 μA respectively, most samples had STD values under 2.7 μA.

Table 6: Average Icorr and STD values obtained from GP readings for FA single rebar specimens.

FA mix			
Sample Name	**Reservoir Length (cm)**	**Avg. Icorr (μA)**	**STD (μA)**
FA-1	5	4.6	2.0
FA-2		10.9	3.9
FA-3		5.7	1.1
FA-4	7.5	12.6	5.2
FA-5		11.0	2.3
FA-6		10.0	2.9
FA-7	17.5	8.2	1.4
FA-8*		-	-
FA-9*		-	-
FA-10	2.5	5.5	0.9
FA-11		3.0	0.5

Note: (*) stands for those specimens that had been terminated

Source: Authors.

In the laboratory experiment by Otieno et al. [7], notable differences were found in the corrosion behavior of concrete samples made with 50% GGBS (SL) and 30% fly ash (FA). The experiment used specimens with a w/cm ratio of 0.40 and cover depths of 40 mm and 20 mm. An accelerated corrosion test was conducted, involving a 7-day cycle: 3 days of exposure to a 5% NaCl solution and 4 days of air drying, at a controlled temperature of 25 ± 2 °C and 50 ± 5% relative humidity. To stimulate corrosion, an anodic impressed current was applied, assuming corrosion over the entire exposed steel surface area of 86 cm^2. At the time of data collection, the specimens were approximately 854 days old. Results showed that SL specimens with 40 mm cover had an average Icorr of 32.7 μA, while those with 20 mm cover had 44.7 μA [7]. In contrast, FA specimens with 40 mm cover showed a much higher Icorr of 91.2 μA, and those with 20 mm cover had 49.9 μA [7]. Otieno et al.'s study revealed that all the specimens were experiencing considerable

active corrosion.

Table 7: Average Icorr and STD values obtained from GP readings for T1 & T2 single rebar specimens.

T1 & T2 mixes			
Sample Name	**Reservoir Length (cm)**	**Avg. Icorr (μA)**	**STD (μA)**
T1-7	5	7.1	2.6
T1-10		3.3	0.8
T1-9	10	15.2	5.7
T1-6*	15	-	-
T1-8		9.5	4.0
T2-1	5	6.7	2.6
T2-3		4.3	1.1
T2-5		3.0	0.7
T2-4*	10	-	-
T2-2	15	10.0	3.2
T2-11		6.4	2.0

Note: (*) stands for those specimens that had been terminated

Source: Authors.

Hope and Ip experimented on SL samples consisting of a 50% slag and 50% Portland cement (PC) mix, with a w/cm ratio of 0.45 and a 56 mm cover depth [41]. The specimens underwent wetting and drying cycles, where they were submerged in a 3.5% NaCl solution and then exposed to laboratory air to promote chloride penetration. It was assumed that the entire exposed steel surface area of 102 cm^2 was corroding. During the first 200 days, the average Icorr was around 51.0 μA. With continued cycles of oven-drying and wetting, this average increased to approximately 61.2 μA between 270 and 315 days [41]. The study concluded that all the specimens showed substantial active corrosion.

O'Reilly et al. conducted laboratory tests on concrete specimens, including SL (20) and SL (40) with 20% and 40% Grade 100 slag cement, and FA (20) and FA (40) with 20% and 40% Class C fly ash [42]. All samples had a w/cm ratio of 0.45 and a cover depth of 25 mm. The experiment involved alternating exposure cycles: 12 weeks of wet-dry cycles followed by 12 weeks of continuous wet cycles. During the wet-dry phase, specimens were ponded with a 15% NaCl solution at room temperature for 4 days, then dried under a heat tent at 100 ± 3 °F (38 ± 2 °C) for 3 days. This process was repeated for 12 weeks. In the next phase, specimens were continuously ponded with a 15% NaCl solution at room temperature for another 12 weeks. It was assumed that a 152 cm^2 steel surface area was corroding. The average Icorr values for SL specimens were 21.0 μA for SL (20) and 13.8 μA for SL (40) [42]. For FA specimens, the average Icorr values were 38.5 μA for FA (20) and 17.6 μA for FA (40) [42]. The specimens were around 672 days (96 weeks) old at the time the data was collected. The study concluded that all the specimens showed substantial active corrosion.

Kayali and Zhu tested a ternary concrete mix containing 23% fly ash and 7% silica fume with a w/cm ratio of 0.35 [43]. Ribbed steel rebar reinforced the specimens, which were partially immersed in a NaCl solution with a chloride ion concentration of 20,000 ppm. It was assumed that the full exposed steel surface area of 177 cm^2 was corroding. The Icorr values for these specimens ranged between 9.7 and 25.3 μA over an exposure period of up to 450 days [43]. The results showed that all specimens exhibited high active corrosion. It is important to mention that in the investigations carried out by Otieno et al., Hope and Ip, O'Reilly et al., as well as Kayali and Zhu, the corrosion current density values reported were converted into Icorr values [7, 41-43]. Similar trends in Icorr values reported in previous studies [44–50] under comparable experimental conditions support the findings of this work and highlight consistent patterns in corrosion behavior across different research efforts.

Figure 8: Variation of average Icorr with length of solution reservoir and concrete mixes cast with single rebar.

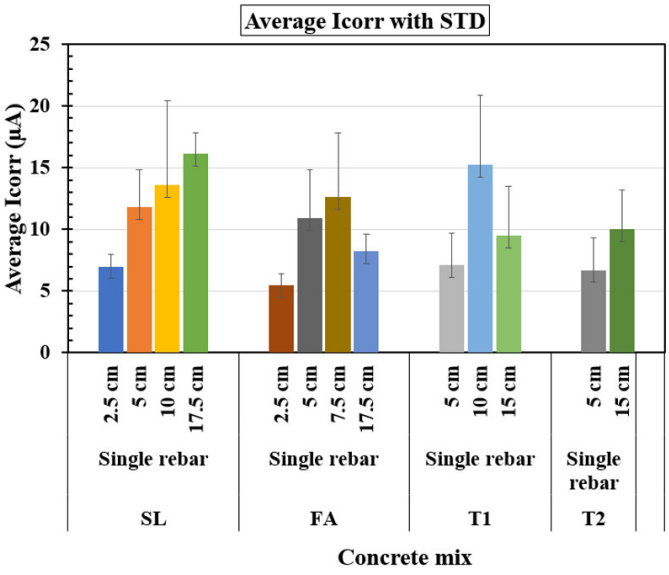

Source: Authors.

It is important to acknowledge that any exposed rebar section outside the concrete, as well as any rebar segment not directly beneath the solution reservoir, could influence corrosion current and other readings (e.g., rebar potential). In some cases, high moisture levels caused the rebar exposed to the atmosphere outside the concrete to corrode. A corroding site, whether embedded or exposed, could provide cathodic protection to the rest of the rebar surface, even in the presence of high chloride levels at the rebar surface. A decrease in current might indicate that the corroding site was less active or that some areas had repassivated, as suggested by the mixed potential values measured at later times. This paper highlights the variation in average Icorr values observed across different concrete mixes (SL, FA, T1, and T2) with single rebar specimens. Fig. 8 provides a graphical summary of the average Icorr variations in relation to the length of the solution reservoir and various concrete mixes. These average Icorr values were obtained from the final 15 sets of readings using the GP method. Generally, Icorr values tended to increase with the length of the solution reservoir for rebars embedded in SL, FA, T1, and T2 concrete mixes. However, some exceptions were noted, such as the FA sample

with a 17.5 cm reservoir and the T1 sample with a 15 cm reservoir, which was also influenced by having only one remaining sample for this reservoir lengths. This trend may be due to the extended length of the solution reservoir, which exposes more of the rebar surface to chlorides, thereby raising the likelihood of corrosion. Additionally, chloride transport continued during the monitoring period. When comparing similar reservoir lengths, rebars in SL concrete mixes generally exhibited higher Icorr values, followed by those in FA, T1, and T2 mixes, indicating that the concrete mix composition significantly influences the corrosion rate.

4.2. Theoretical (Faradaic) calculation of mass loss.

In this study, as none of the samples showed any visible crack, therefore a theoretical mass loss approach was considered. The GP method was performed periodically to get Rc values. The Rc values obtained from GP method were used to be converted into corrosion current. The average corrosion current was calculated from two consecutive Rc values (the average of the two consecutive values for that period). It was then multiplied by the time interval between each measurement to get the total amount of charge, and all calculated charge values were added for each rebar as shown in Eqn. (1). Applying Faraday's law, the apparent mass loss was obtained as shown in Eqn. (2).

$$Q = \sum_{N=1}^{n} \left(\frac{I_N + I_{N-1}}{2} \right) t_N \tag{1}$$

where Q is in coulombs and t is in seconds.

Calculated mass loss by using Faraday's law is given by-

$$Mass\ Loss = Q * Atomic\ Mass / nF \tag{2}$$

where Atomic Mass is 55.85g (for Fe), n is 2 (# of electrons), and F is 96,500 C (Faraday's constant).

Tables 8 to Table 10 present the mass loss values calculated using the GP method. These values, for SL, FA, T1, and T2 single rebar samples, were derived from readings collected over the 1600-day monitoring period.

Tables 8 and Table 9 display the estimated mass loss in grams for SL and FA single rebar samples as determined by the GP method, categorized by the length of the solution reservoir. For SL samples with a 17.5 cm reservoir, the mass loss ranged from 0.14 to 0.50 grams, while for FA samples, it ranged from 0.06 to 0.32 grams. For rebars with a 10 cm reservoir, SL samples showed a mass loss between 0.29 and 0.37 grams, whereas FA samples with a 7.5 cm reservoir had mass losses between 0.38 and 0.47 grams. For the 5 cm reservoir, SL samples mass loss ranged from 0.21 to 0.41 grams, compared to 0.14 to 0.30 grams for FA samples. Lastly, for the 2.5 cm reservoir, SL samples had a mass loss of 0.17 to 0.22 grams, while FA samples ranged from 0.09 to 0.18 grams. In general, mass loss values were quite similar for the 2.5 cm reservoir samples of both type of mixes. However, SL samples showed greater mass loss with 17.5 cm and 10 cm reservoirs, while FA samples had higher mass loss values with 7.5 cm and 5 cm reservoirs.

Table 8: Estimated mass loss in grams obtained from GP readings for SL single rebar samples.

Sample Name	Reservoir length (cm)	Mass loss from GP (grams)
SL-1*	17.5	0.142
SL-2*		0.180
SL-3		0.504
SL-4	2.5	0.176
SL-5		0.216
SL-6	5	0.210
SL-7		0.298
SL-8		0.407
SL-9	10	0.298
SL-10		0.374
SL-11		0.373

Note: (*) stands for those specimens that had been terminated

Source: Authors.

Table 9: Estimated mass loss in grams obtained from GP readings for FA single rebar samples.

Sample Name	Reservoir length (cm)	Mass loss from GP (grams)
FA-1	5	0.135
FA-2		0.290
FA-3		0.300
FA-4	7.5	0.472
FA-5		0.381
FA-6		0.432
FA-7	17.5	0.316
FA-8*		0.056
FA-9*		0.105
FA-10	2.5	0.180
FA-11		0.093

Note: (*) stands for those specimens that had been terminated

Source: Authors.

Table 10 presents the estimated mass loss in grams for T1 and T2 single rebar samples, as determined by the GP method, based on the length of the solution reservoir. For T1 samples with a 15 cm reservoir, the mass loss ranged from 0.24 to 0.36 grams, while for T2 samples, it ranged from 0.17 to 0.29 grams. With a 10 cm reservoir, T1 samples had a mass loss of 0.49 grams compared to 0.06 grams for T2 samples. For a 5 cm reservoir, T1 samples showed a mass loss between 0.12 and 0.22 grams, whereas T2 samples ranged from 0.10 to 0.21

grams. It was observed that T1 samples had higher mass loss with 15 cm and 10 cm reservoirs, whereas T2 samples experienced greater mass loss with 15 cm and 5 cm reservoirs.

Fig. 9 summarizes how average mass loss values vary with solution reservoir length and concrete mix type, each containing a single rebar. These values, calculated from GP method readings over roughly 1600 days, generally showed that longer reservoirs led to higher average mass loss for rebars in SL, FA, T1, and T2 mixes. However, exceptions were observed for SL and FA samples with 17.5 cm reservoirs, T1 samples with 15 cm reservoirs, and T2 samples with 10 cm reservoirs. Notably, four samples (SL-1, SL-2, FA-8, and FA-9) with 17.5 cm reservoirs and two samples (T1-6 and T2-4) with 15 cm and 10 cm reservoirs were terminated early for forensic analysis. Consequently, the average mass loss values for these samples were lower than what would have been recorded had they not been terminated.

Table 10: Estimated mass loss in grams obtained from GP readings for T1 and T2 single rebar samples.

Sample Name	Reservoir length (cm)	Mass loss from GP (grams)
T1-7	5	0.222
T1-10		0.120
T1-9	10	0.493
T1-6*	15	0.240
T1-8		0.360
T2-1	5	0.209
T2-3		0.145
T2-5		0.100
T2-4*	10	0.062
T2-2	15	0.298
T2-11		0.173

Note: (*) stands for those specimens that had been terminated

Source: Authors.

Torres-Acosta conducted an experimental study involving two types of specimens: concrete beam specimens and concrete cylindrical specimens reinforced with carbon steel rebar [51]. In the preparation process, chlorides were introduced into the concrete mix of these specimens. All specimens were exposed to a relative humidity (RH) of 75%. To induce corrosion, an impressed current of 100 μA/cm^2 was applied. For the concrete beam specimens, the observed mass loss values, determined through forensic analysis, ranged from 0.3 to 14.4 grams. Faradaic calculations yielded similar values, ranging from 0.3 to 12.5 grams. In the case of the concrete cylindrical specimens undergoing corrosion, mass loss values were determined to be between 0.7 and 5.1 grams through gravimetric analysis and between 0.6 and 5.8 grams through Faradaic calculation. It was reported in Torres-Acosta's study that the calculated mass loss values, representing the amount of corrosion products, led to the development of cracks in all the specimens [51]. However, in the current investigation, no cracks were observed through visual inspection. In the current study, the moisture content was higher than in Torres-Acosta study. Additionally, the mass loss in the current study likely includes some of the rebar corrosion that took place outside the concrete.

Figure 9: Variation of mass loss (GP) with length of solution reservoir and concrete mixes cast with single rebar .

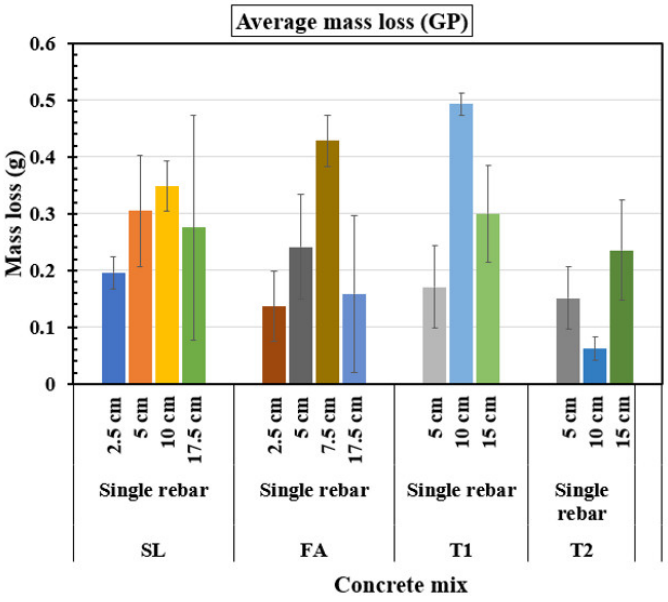

Source: Authors.

Balasubramanian conducted an experimental study on reinforced concrete pipe sections with two different concrete mixes [52]. One mix incorporated fly ash, replacing 20% of the cement, while the other used ordinary Portland cement. No chlorides were added during specimen preparation. The specimens were exposed to various environmental conditions and subjected to an electromigration technique to induce corrosion [52]. For specimens with fly ash in a high humidity environment (95% RH at 21ºC), mass loss ranged from 2.0 to 10.3 grams according to forensic analysis and from 1.9 to 11.3 grams based on Faradaic calculations. For ordinary Portland cement specimens in the same high humidity conditions, mass loss values were between 0.6 and 3.2 grams through forensic analysis and 1.0 to 3.9 grams through Faradaic calculations. In vertically exposed fly ash specimens, mass loss varied from 0.6 to 1.2 grams (forensic analysis) and 2.0 to 5.9 grams (Faradaic calculation). Horizontally exposed fly ash specimens showed mass loss values from 0.1 to 0.3 grams (forensic analysis) and 1.9 to 2.0 grams (Faradaic calculation). The current study did not determine the exact size of the corroding sites, as many specimens were not analyzed for forensic purposes. The amount of corrosion products needed to cause concrete cracking may depend on the size of these corroding sites. Under the reservoir, corrosion regions were noted, with corrosion products penetrating the concrete by

several millimeters [52]. Forensic analysis revealed localized corrosion in most specimens, and while the exposed reinforcement area was larger than the corroding area, no cracks were observed in Balasubramanian's study [52]. It is suggested that smaller corroding sites might need a larger amount of mass loss to cause concrete cover cracking. The high moisture content in the concrete may allow corrosion products to spread more broadly, rather than concentrating the force in one location. No visible cracks or corrosion bleed-outs were noted, possibly because the corrosion products migrated through the concrete's pore structure, settling away from the reinforcing surface within the concrete cover. Very small corroding sites and relatively moderate cross-sectional loss were observed in the few specimens that were terminated [36, 37, 53, 54].

5. General Discussion

In this study, the electromigration technique was employed to expedite chloride transport. This method involved applying an electric field to drive chlorides from the solution reservoir into the concrete, targeting the embedded rebar. Consequently, corrosion of the rebar initiated relatively swiftly, often within weeks or months. Corrosion initiation was monitored by measuring rebar potential and corrosion current values. Interestingly, a further decline in rebar potential was observed several weeks after the electromigration was halted. This technique successfully induced corrosion either immediately or after a delay post-electromigration, as evidenced by rebar potential values shifting to more negative than -0.200 Vsce for most samples.

During the observation of corrosion propagation, GP tests proved effective in monitoring changes in Icorr values. Fluctuations in Icorr values were noted during the corrosion progression phase. It was hypothesized that some rebar sections might have repassivated, or that non-corroding sections influenced the polarization of corroding areas. Additionally, corrosion occurring outside the concrete could have impacted these readings.

After suspending the electromigration for several months, various Icorr transients were noted. These transients could be influenced by factors such as concrete composition, reservoir length, total ampere-hours applied, and environmental conditions like moisture, oxygen availability, and relative humidity.

The specimens, designated SL, FA, T1, and T2, were kept in a high-humidity indoor laboratory environment. Initially, parts of the rebar extended beyond the concrete and were not covered with shrinkage wrap. The high humidity led to moisture droplets on the exposed rebar, potentially causing corrosion of the outer sections. Instances of solution overflow from the reservoir reaching the rebar, but not within the concrete, could also contribute to corrosion and affect the Icorr readings. To address this, the exposed rebar sections were cleaned and sealed with shrinkage wrap 500 days after the electromigration phase. Post-intervention, electrochemical measurements showed improved consistency. As time progressed, crevice corrosion may have occurred beneath the shrinkage wrap.

Angst and collaborators observed that, in some cases of chloride-induced corrosion, there were no visible signs such as rust stains or cracks. However, detailed forensic analysis revealed significant cross-sectional loss at the corrosion sites [55]. They argued that the widely accepted model, which assumes corrosion occurs evenly around the entire rebar, is not adequate for explaining the actual corrosion process [55]. First, iron dissolution tends to be localized rather than uniform around and along the rebar. Second, due to the presence of chlorides, corrosion products are more soluble and less likely to precipitate near the corroding area. Third, chloride-induced corrosion often begins at weak points in the steel/concrete interface, like areas of higher porosity, which can hinder the buildup of expansive pressure. Angst's study documented instances where chloride-induced corrosion led to significant cross-sectional loss without noticeable surface stains [55]. Similar findings were observed during the termination of some samples in this research [36, 37, 53, 54].

Conclusions.

In this study, the electromigration method was used to accelerate chloride transport, leading to the initiation of corrosion within just a few weeks to a few months.

The corrosion current values, measured electrochemically, were significantly influenced by environmental conditions and the length of the solution reservoirs used in the different concrete mixes. Generally, for most rebars embedded in the concrete specimens, an increase in the length of the solution reservoir resulted in higher corrosion current values, although there were some exceptions to this pattern.

For the single rebar specimens, the average corrosion current values (based on the last 15 sets of readings) were highest for rebars embedded in specimens made with the SL mix, followed by those made with FA, T1, and T2 mixes, in that order. The ranges of corrosion current values were 5.6-16.1 μA for SL samples, 3.0-12.6 μA for FA samples, 3.3-15.2 μA for T1 samples, and 3.0-10.0 μA for T2 samples, respectively.

It was also noted that rebars with larger reservoir sizes generally had higher calculated mass loss values. The mass loss values calculated from the GP readings ranged between 0.14-0.50 grams for SL samples, 0.06-0.47 grams for FA samples, 0.12-0.49 grams for T1 samples, and 0.06-0.30 grams for T2 samples, respectively.

No visible signs of corrosion, such as cracks or rust stains, were observed on the top surface of the specimens. Since most specimens were not terminated for forensic analysis, the actual size of the corroding sites remained unknown. The extent of the corroding sites could influence how much corrosion product is needed to crack the concrete. It is speculated that in the high-moisture condition of the concrete, corrosion products in liquid form penetrated the pore structure without creating concentrated bursting forces in a single location. Throughout the monitored propagation period of approximately 1600 days, no cracks or corrosion bleed-outs were observed.

Conflict of Interest.

The authors declare no conflict of interest.

Acknowledgements.

The authors gratefully acknowledge the Florida Department of Transportation (FDOT) for their support in preparing the samples. The authors acknowledge the financial support provided by the FDOT (Grant No. BDV 27-977-08 FAU# AWD-000917) and the TriDurLE (Grant No. FAU# AWD-002175). The authors extend their gratitude to Florida Atlantic University and sincerely thank the graduate and undergraduate students from the Marine Materials and Corrosion Laboratory at FAU for their assistance with laboratory work and data collection. The opinions expressed in this paper are solely those of the authors and do not necessarily reflect the views of FAU, FDOT, or TriDurLE.

References.

1. Angst UM (2018) Challenges and opportunities in corrosion of steel in concrete. Mater. Struct., vol. 51(4), pp. 1–20.

2. Jones AEK (1997) Development of a holistic approach to ensure the durability of new concrete construction. British Cement Association, Crowthorne.

3. fib-Model-Code (2010) 3rd FIP/CEB Model Code for concrete structures. Comite Euro-International du Beton and Federation International de Precontrainte.

4. Broomfield JP (2007) Corrosion of steel in concrete-understanding, investigation and repair, 2nd edition. Taylor & Francis, Oxford.

5. Castel A, Vidal T, Francois R, Arliguie G (2003) Influence of steel-concrete interface quality on reinforcement corrosion induced by chlorides. Mag. Concr. Res., vol. 55(2), pp. 151-160.

6. Francois R, Arliguie G (1998) Influence of service cracking on reinforcement steel corrosion. J. Mater. Civ. Eng., vol. 10(1), pp. 14-20.

7. Otieno M, Beushausen H, Alexander M (2016) Chloride-induced corrosion of steel in cracked concrete-part I: experimental studies under accelerated and natural marine environments. Cem. Concr. Res., vol. 79, pp. 373-385.

8. Vidal T, Castel A, Francois R (2007) Corrosion process and structural performance of a 17-year-old reinforced concrete beam stored in chloride environment. Cem. Concr. Res., vol. 37(11), pp. 1551-1561.

9. Zhang R, Castel A, Francois R (2009) Serviceability limit state criteria based on steel-concrete bond loss for corroded reinforced concrete in chloride environment. Mater. Struct., vol. 42(10), pp. 1407-1421.

10. Zhang R, Castel A, Francois R (2009) The corrosion pattern of reinforcement and its influence on serviceability of reinforced concrete members in chloride environment. Cem. Concr. Res., vol. 39(11), pp. 1077-1086.

11. Zhang R, Castel A, Francois R (2010) Concrete cover cracking with reinforcement corrosion of RC beam during chloride-induced corrosion process. Cem. Concr. Res., vol. 40(3), pp. 415-425.

12. Ballim Y, Reid JC (2003) Reinforcement corrosion and the deflection of RC beams-an experimental critique of current test methods. Cement Concr. Compos., vol. 25(6), pp. 625-632.

13. El Maaddawy T, Soudki K (2007) A model for prediction of time from corrosion initiation to corrosion cracking. Cement Concr. Compos., vol. 29(3), pp. 168-175.

14. Liu Y, Weyers RE (1998) Modelling the time-to-corrosion cracking in chloride contaminated reinforced concrete structures. ACI Mater. J., vol. 95(6), pp. 675-681.

15. Malumbela G, Moyo P, Alexander MG (2009) Behaviour of reinforced concrete beams under sustained service loads. Constr Build. Mater., vol. 23(11), pp. 3346-3351.

16. Torres-Acosta AA, Fabela-Gallegos MJ, Munoz-Noval A, Vazques-Vega D, Hernandez-Jimenez JR (2004) Influence of corrosion on the structural stiffness of reinforced concrete beams. Corrosion, vol. 60(9), pp. 862-872.

17. Torres-Acosta AA, Navarro-Guitierrez S, Teran-Guillen J (2007) Residual flexure capacity of corroded reinforced concrete beams. Eng. Struct., vol. 29(6), pp. 1145-1152.

18. El Maaddawy T, Soudki KA (2003) Effectiveness of impressed current technique to simulate corrosion of steel reinforcement in concrete. ASCE J. Mater. Civ. Eng., vol. 15(1), pp. 41-47.

19. Polder RB, Peelen HA (2002) Characterization of chloride transport and reinforcement corrosion in concrete under cyclic wetting and drying by electrical resistivity. Cem. Concr. Compos., vol. 24, pp. 427-435.

20. Wu J, Li H, Wang Z, Liu J (2016) Transport model of chloride ions in concrete under loads and drying-wetting cycles. Constr. Build. Mater., vol. 112, pp. 733-738.

21. Ye H, Jin X, Fu C, Jin N, Xu Y, Huang T (2016) Chloride penetration in concrete exposed to cyclic drying-wetting and carbonation. Constr. Build. Mater., vol. 112, pp. 457-463.

22. Jung WY, Yoon YS, Sohn YM (2003) Predicting the remaining service life of land concrete by steel corrosion. Cem. Concr. Res., vol. 33(5), pp. 663-677.

23. Otieno MB, Beushausen HD, Alexander MG (2016) Chloride-induced corrosion of steel in cracked concrete-part II: corrosion rate prediction models. Cem. Concr. Res., vol. 79, pp. 386-394.

24. Andrade C, Alonso C, Molina FJ (1993) Cover Cracking as a Function of Rebar Corrosion: Part I -Experimental Test. Materials and Structures, vol. 26, pp. 453-464.

25. Alonso C, Andrade C, Rodriguez J (1998) Factors Controlling Cracking of Concrete Affected by Reinforcement Corrosion. Materials and Structures, vol. 31, pp. 435 -441.

26. Andrade C, Alonso C, Rodriguez J, Garcia M (1996) Cover Cracking and Amount of Rebar Corrosion: Importance of the Current Applied Accelerated Tests. Concrete Repair, Rehabilitation and Protection, R. K. Dhir and M. R. Jones, eds., E&FN Spon, London, pp. 263-273.

27. Rasheeduzzafar, Al-Saadoun SS, Al-Gahtani AS (1992) Corrosion Cracking in Relation to Bar Diameter, Cover, and Concrete Quality. Journal of Materials in Civil Engineering, ASCE, vol. 4(4), pp. 327-342.

28. Saeki N, Fujita Y, Takada N, Ohta T (1988) Control of Rust Damage of Reinforced Concrete in a Corrosive Environment. Concrete in Marine Environment, Proceedings of the

Second International Conference, SP-109, V. M. Malhotra, ed., American Concrete Institute, Farmington Hills, Mich., pp. 163-177.

29. Torres-Acosta A, Sagüés AA (2004) Concrete Cracking by Localized Steel Corrosion-Geometric Effects. ACI Materials Journal, vol. 101(6), pp. 501-507.

30. Busba E, Sagüés AA (2013) Critical Localized Corrosion Penetration of Steel Reinforcement for Concrete Cover Cracking, CORROSION/2013, paper no. C2013-0002747 (Houston, TX).

31. Otieno M, Beushausen H, Alexander M (2012) Prediction of corrosion rate in reinforced concrete structures-a critical review and preliminary results. Materials and Corrosion, vol. 63(9), pp. 777-790.

32. Otieno MB, Alexander MG, Beushausen H (2010) Corrosion in cracked and uncracked concrete-influence of crack width, concrete quality and crack reopening. Magazine of Concrete Research, vol. 62(6), pp. 393-404.

33. Vidal T, Castel A, Francois R (2004) Analyzing crack width to predict corrosion in reinforced concrete. Cement and Concrete Research, vol. 34, pp. 165-174.

34. Presuel-Moreno F, Balasubramanian H, Wu Y (2013) Corrosion of reinforced concrete pipes: an accelerated approach. Corrosion 2013, paper no. C2013-0002551 (Houston, TX).

35. Hoque K (2020) Corrosion propagation of reinforcing steel embedded in binary and ternary concrete. Ph.D. Dissertation, Department of Ocean and Mechanical Engineering, Florida Atlantic University (FAU), Boca Raton, Florida, USA.

36. Presuel-Moreno F, Hoque K (2019) Corrosion propagation of carbon steel rebar embedded in concrete. Corrosion 2019, Nashville, Tennessee, USA.

37. Presuel-Moreno F, Nazim M, Tang F, Hoque K, Bencosme R (2018) Corrosion Propagation of Carbon Steel Rebars in High Performance Concrete. BDV27-977-08 Final Report for FDOT.

38. Andrade C, Alonso C (1996) Corrosion rate monitoring in the laboratory and on-site. Constr. Build. Mater., vol. 10(5), pp. 315-328.

39. Feliu V, Gonzalez JA, Feliu S (2007) Corrosion estimates from transient response to a potential step. Corros. Sci., vol. 49(8), pp. 3241-3255.

40. Gonzalez JA, Miranda JM, Feliu S (2004) Consideration on the reproducibility of potential and corrosion rate measurements in reinforced concrete. Corros. Sci., vol. 46(10), pp. 2467-2485.

41. Hope BB, Ip AKC (1987) Corrosion of steel in concrete made with slag cement. ACI Materials Journal, vol. 84(6), pp. 525-531.

42. O'Reilly M, Omid F, Darwin D (2019) Effect of Supplementary Cementitious Materials on Chloride Threshold and Corrosion Rate of Reinforcement. ACI Materials Journal, Title No. 116-M12, pp. 125-133.

43. Kayali O, Zhu B (2005) Chloride induced reinforcement corrosion in lightweight aggregate high strength ?y ash concrete. Construction and Building Materials, vol. 19, pp. 327-336.

44. Hoque KN, Presuel-Moreno F (2023) Accelerated Corrosion of Steel Rebar in Concrete by Electromigration: Effect of Reservoir Length and Concrete Mixes. Proceedings of the 13th International Conference on Marine Technology (MARTEC 2022).

45. Hoque KN, Presuel-Moreno F (2023) Corrosion Propagation of Steel Rebar Embedded in Marine Structures Prepared with Binary Blended Concrete Containing Slag. Proceedings of the 13th International Conference on Marine Technology (MARTEC 2022).

46. Presuel-Moreno F, Hoque K, Rosa-Pagan A (2022) Corrosion propagation monitoring using galvanostatic pulse on reinforced concrete legacy samples. 2020-FAU-02 Final Report for National University Transportation Center TriDurLE.

47. Hoque KN, Presuel-Moreno F (2023) Corrosion Behaviour of Reinforcing Steel Embedded in Fly Ash Concrete. Proceedings of the 13th International Conference on Marine Technology (MARTEC 2022).

48. Hoque KN, Presuel-Moreno F (2023) Corrosion of Steel Rebar Embedded in Ternary Blended Concrete Exposed to High Humidity Environment. Proceedings of the 13th International Conference on Marine Technology (MARTEC 2022).

49. Hoque KN, Presuel-Moreno F (2024) Electromigration-Based Investigation of Corrosion Behaviour in Ternary Blended Reinforced Concrete. International Journal of Structural and Civil Engineering Research, vol. 13(3), pp. 90-95.

50. Hoque KN, Presuel-Moreno F (2024) Chloride-induced corrosion of reinforcing steel embedded in ternary blended concrete. Journal of Naval Architecture and Marine Engineering, vol. 21(2), pp. 195–206.

51. Torres-Acosta AA (1999) Cracking Induced by Localized Corrosion of Reinforcement in Chloride Contaminated Concrete. Ph.D. Dissertation, Department of Civil & Environmental Engineering, University of South Florida.

52. Balasubramanian H (2019) Initiation and Propagation of Corrosion in Dry cast Reinforced Concrete Pipes with Environmental Effects. Ph.D. Dissertation, Department of Ocean & Mechanical Engineering, Florida Atlantic University.

53. Hoque KN, Presuel-Moreno F, Nazim M (2023) Corrosion of carbon steel rebar in binary blended concrete with accelerated chloride transport. Journal of Infrastructure Preservation and Resilience, vol. 4(26), pp. 1-15.

54. Hoque KN, Presuel-Moreno F, Nazim M (2023) Accelerated Electromigration Approach to Evaluate Chloride-Induced Corrosion of Steel Rebar Embedded in Concrete. Advances in Materials Science and Engineering, Article ID. 6686519, pp. 1-14.

55. Angst UM, Elsener B, Jamali A, Adey B (2012) Concrete cover cracking owing to reinforcement corrosion-theoretical considerations and practical experience. Materials and Corrosion, vol. 63(12), pp. 1069-1077.